



Crustal structure and evolution beneath the Colorado Plateau and the southern Basin and Range Province: Results from receiver function and gravity studies

Lamuail Bashir, Stephen S. Gao, and Kelly H. Liu

Department of Geological Sciences and Engineering, Missouri University of Science and Technology, Rolla, Missouri 65409, USA (lbvd3@mst.edu; sgao@mst.edu; liukh@mst.edu)

Kevin Mickus

Department of Geography, Geology, and Planning, Missouri State University, Springfield, Missouri 65897, USA (kevinmickus@missouristate.edu)

[1] Over the past several decades, contrasting models have been proposed for the physical and chemical processes responsible for the uplift and long-term stability of the Colorado Plateau (CP) and crustal thinning beneath the Basin and Range Province (BRP) in the southwestern United States. Here we provide new constraints on the models by modeling gravity anomalies and by systematically analyzing over 15,500 *P*-to-*S* receiver functions recorded at 72 USArray and other broadband seismic stations on the southwestern CP and the southern BRP. Our results reveal that the BRP is characterized by a thin crust (28.2 ± 0.5 km), a mean V_p/V_s of 1.761 ± 0.014 and a mean amplitude (R) of *P*-to-*S* converted wave (relative to that of the direct *P* wave) of 0.181 ± 0.014 that are similar to a typical continental crust, consistent with the model that the thin crust was the consequence of lithospheric stretching during the Cenozoic. The CP is characterized by the thickest crust (42.3 ± 0.8 km), largest V_p/V_s (1.825 ± 0.009) and smallest R (0.105 ± 0.007) values in the study area. In addition, many stations on the CP exhibit a clear arrival before the *P*-to-*S* converted phase from the *Moho*, corresponding to a lower crustal layer of about 12 km thick with a mafic composition. We hypothesize that the lower crustal layer, which has an anomalously large density as revealed by gravity modeling and high velocities in seismic refraction lines, contributed to the long-term stability and preuplift low elevation of the Colorado Plateau.

Components: 13,900 words, 11 figures, 1 table.

Keywords: Basin and Range Province; Bouguer gravity; Colorado Plateau; continental crust; receiver function.

Index Terms: 7203 Seismology: Body waves; 7205 Seismology: Continental crust (1219); 8110 Tectonophysics: Continental tectonics: general (0905).

Received 15 February 2011; **Accepted** 18 April 2011; **Published** 22 June 2011.

Bashir, L., S. S. Gao, K. H. Liu, and K. Mickus (2011), Crustal structure and evolution beneath the Colorado Plateau and the southern Basin and Range Province: Results from receiver function and gravity studies, *Geochem. Geophys. Geosyst.*, 12, Q06008, doi:10.1029/2011GC003563.

1. Introduction

[2] The southwestern portion of the United States has undergone a series of tectonic events ranging from

Proterozoic orogenesis [Whitmeyer and Karlstrom, 2007; Karlstrom and Bowring, 1988], flat subduction of the Farallon plate in the late Cretaceous to early Tertiary [Saleeby, 2003] creating widespread

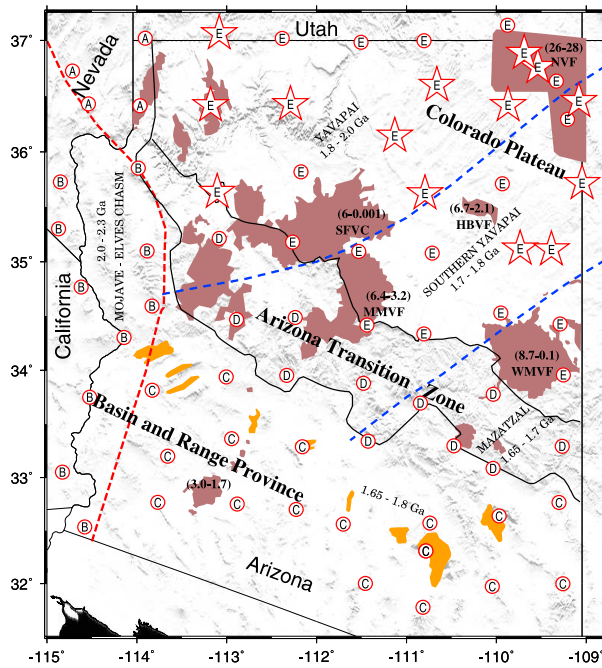


Figure 1. Major geologic provinces and their ages [Bennett and DePaolo, 1987; Livaccari and Perry, 1993], volcanic fields (brown areas) and their ages, metamorphic core complexes (orange areas) [Hendricks and Plescia, 1991], and location of seismic stations (open circles and stars) used in this study. Stars indicate stations showing a secondary arrival between the direct P wave and the P -to- S converted phase from the Moho. The letter inside each of circles represents the tectonic area based on seismic and surface geology analyses. Area A, a transition zone between the CP and the eastern portion of the BRP north of Grand Canyon; area B, Mojave-Elves Chasm; area C, the BRP in southern Arizona; area D, Arizona transition zone; area E, Colorado Plateau. The red dashed line separates the highly extended terrane with older Proterozoic rocks in the Mojave Desert and less extended terrane and younger Proterozoic rocks in central Arizona [Wooden and DeWitt, 1991; Bennett and DePaolo, 1987]. The blue dashed lines represent the suture between the Yavapai, southern Yavapai, and Mazatzal provinces [Bennet and DePaolo, 1987; Karlstrom and Humphreys, 1998; Selverstone et al., 1999]. The black solid lines outline the Arizona Transition Zone [Hendricks and Plescia, 1991]. The major volcanic fields in the study area include the Navajo (NVF), San Francisco (SFVC), Hopi Buttes (HBVF), White Mountains (WMVF), and Mormon mountain volcanic fields (MMVF) [Hendricks and Plescia, 1991; Condie and Selverstone, 1999].

magmatism and crustal shortening, Cenozoic uplift of the Colorado Plateau (CP) [Liu and Gurnis, 2010] to the Late Cenozoic extension within the Basin and Range Province (BRP) [Menges and Peartree, 1989]. A majority of the above tectonic events can be

observed in Arizona where the CP and BRP dominate the present day tectonic environment (Figure 1). Major features with a sharp contrast between the two provinces include surface elevation, heat flow, crustal thickness, tectonic deformation, Bouguer gravity, and crustal Poisson's ratio [e.g., Thompson and Zoback, 1979; Sumner, 1989; Frassetto et al., 2006; Gilbert et al., 2007].

[3] Numerous active-source seismic refraction/reflection studies (Figure 2) suggest that crustal thickness (H) ranges from 40 to 50 km beneath the CP, and 28–32 km beneath the BRP [Roller, 1965; Warren, 1969; Prodehl, 1979; Gish et al., 1981; Sinno et al., 1981; Hauser and Lundy, 1989; McCarthy et al., 1991; Wolf and Cipar, 1993; Parsons et al., 1996]. Similar results were obtained by applying the receiver function (RF) method to broadband seismic data [Zandt et al., 1995; Wilson et al., 2005; Frassetto et al., 2006; Gilbert et al., 2007; Wilson et al., 2010]. These studies have proposed crustal evolution models mainly based on crustal thickness but some of the studies [e.g., Frassetto et al., 2006; Gilbert et al., 2007] used V_p/V_s measurements in determining the nature of the crust and hence the tectonic history.

[4] The gravity field of the study area has been studied by numerous researchers [e.g., Aiken, 1976; Keller et al., 1979; Thompson and Zoback, 1979; Sumner, 1989; Hendricks and Plescia, 1991]. These workers have shown that there is an excellent correlation between the tectonic provinces (CP and BRP) and Bouguer gravity anomalies. The CP has high amplitude negative Bouguer gravity values that correspond to thicker crust and lithosphere, and has Free-air gravity values that average to approximately 0 mGal implying that it is in isostatic equilibrium [Aiken, 1976; Thompson and Zoback, 1979]. The BRP has relatively high amplitude Bouguer gravity values which agree with the thinner crust found in the region [McCarthy et al., 1991]. Two-dimensional regional gravity models [Thompson and Zoback, 1979; Mickus, 1989; Hendricks and Plescia, 1991] constrained by seismic refraction models [e.g., Warren, 1969; McCarthy et al., 1991] indicate that crust beneath the BRP is thinner with a less dense upper mantle than that under the CP, and that there is a steep gradient in crustal thicknesses between the two provinces. Detailed gravity modeling [McCarthy et al., 1991; Mickus and James, 1991] along a seismic refraction profiles in western Arizona indicates that the lower crust is significantly denser and thicker in narrow regions associated with highly extended crustal regions.

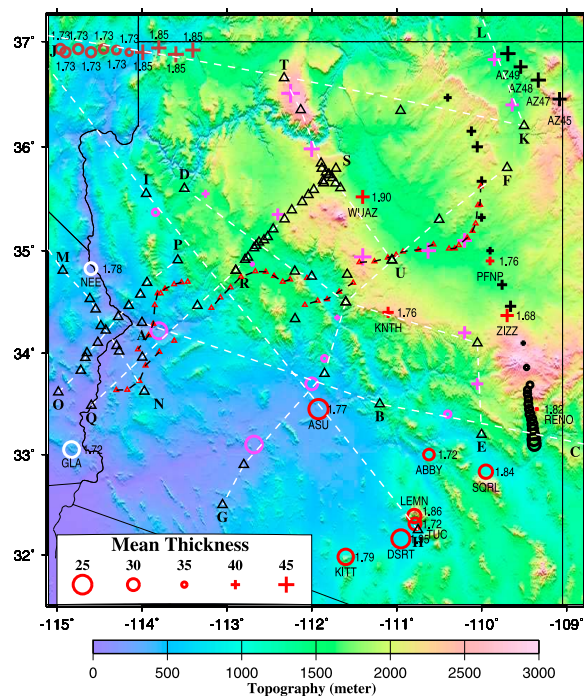


Figure 2. Topographic map of the study area showing previous determinations of crustal thickness and V_p/V_s . Dashed white lines connecting black triangles are seismic refraction surveys [Sinno *et al.*, 1981; Wilson and Fuis, 1987]. Triangles denote shot points. AB, Sinno *et al.* [1981]; BC, Gish *et al.* [1981]; DE and FG, Warren [1969]; JI, Diment *et al.* [1961]; JH, Langston and Helmberger [1974] and Bache *et al.* [1978]; EK, Bache *et al.* [1978]; KL, Roller [1965]; MN and OP, Wilson and Fuis [1987]; QR, instrument deployment of the PACE 1987; QS, profile of PACE 1989 [McCarthy *et al.*, 1994]; TU, Grand Canyon profile of PACE 1989 [McCarthy *et al.*, 1994]. Black dotted lines joined by red triangles are COCORP deep seismic reflection profiles [Hauser *et al.*, 1987]. The pink pluses and circles indicate the average crustal thickness along seismic refraction and reflection profiles [Roller, 1965; Warren, 1969; Hauser and Lundy, 1989; Wolf and Cipar, 1993; Parsons *et al.*, 1996]. Red circles and pluses indicate crustal thickness determined by Frassetto *et al.* [2006] using receiver functions. Black circles and pluses represent crustal thickness from Gilbert *et al.* [2007]. Brown circles and pluses are those from Zandt *et al.* [1995], and white circles show results of Zhu and Kanamori [2000]. The numbers next to the circles or pluses are V_p/V_s determinations. Note that in order to highlight spatial variations of the crustal parameters such as thickness, throughout the text greater values are represented by bigger pluses, and smaller values are shown as bigger circles (see the legend).

[5] Recent developments in RF studies revealed that in addition to crustal thickness, the V_p/V_s measurement, which is uniquely related to the better-known Poisson's ratio (σ) by $\sigma = 0.5 [1 - 1/$

$(\phi^2 - 1)]$, where $\phi = V_p/V_s$, provides additional information on crustal composition and evolution [e.g., Zhu and Kanamori, 2000; Nair *et al.*, 2006; Liu and Gao, 2010]. Laboratory experiments suggest that the average V_p/V_s value for granitic, andesitic, and basaltic rocks is 1.71, 1.78, and 1.87, respectively [Tarkov and Vavakin, 1982], and that for the upper crust and lower crust, V_p/V_s is 1.74 and 1.81, respectively [Christensen, 1996]. Previous RF studies in the study area suggest that V_p/V_s values range from 1.81 to 1.90 in the CP and from 1.73 to 1.78 in the BRP [Zandt *et al.*, 1995; Frassetto *et al.*, 2006; Gilbert *et al.*, 2007] (Figure 2).

[6] The present study is motivated by a number of factors. First, the previous RF studies in the area have limited number of stations, and the station distribution was uneven (Figure 2). Second, a different set of crustal thickness and V_p/V_s measuring techniques and crustal velocities were used in previous studies, which led to a heterogeneous data set that makes inter-station comparisons unreliable. For instance, Zandt *et al.* [1995] used a P wave velocity of 6.25 km/s and a constant V_p/V_s of 1.73 V_p/V_s when computing crustal thickness, while Frassetto *et al.* [2006] used a P wave velocity of 6.1–6.3 km/s; Gilbert *et al.* [2007] used a P -wave velocity of 6.475 km/s and a V_p/V_s of 1.81 for LA RISTRA and 1.85 for SPE stations. Third, virtually none of the previous studies conducted in-depth investigations of the stacking amplitude (R) of the P -to- S converted phases and their multiples. As demonstrated in recent studies [Nair *et al.*, 2006; Liu and Gao, 2010], the stacking amplitude is effective in providing additional information about the structure and evolution of the crust, especially in areas with potentially magmatic underplating and other forms of magmatic modification of the original crust. Finally, this study takes the advantage of the high-quality data recorded by the nearly evenly distributed EarthScope Transportable Array (TA) stations to comprehensively investigate the spatial distribution of H , V_p/V_s , and R in Arizona, where a sharp contrast in crustal characteristics between the CP and the BRP has been previously noted [Sumner, 1989], but the nature and cause(s) of such contrast have been debated, mostly due to a lack of detailed knowledge about crustal characteristics beneath the CP and the BRP.

2. Tectonic Setting

[7] Proterozoic terranes in the study area include the Mojave-Elves Chasm, Yavapai, southern Yavapai,

and the Mazatzal provinces (Figure 1) [Whitmeyer and Karlstrom, 2007]. The oldest rocks found in the study area are Proterozoic granitoids and gneisses with an estimated age ranging from 2.0 to 2.3 Ga found in the Mojave-Elves Chasm terrane (area B, Figure 1) [Bennett and DePaolo, 1987]. Proterozoic tectonic events, which created the northeasterly trending Yavapai and Mazatzal terranes, involved a series of tectonic pulses including accretion, back-arc spreading and continental margin volcanic arcs from 1.6 to 1.8 Ga [Whitmeyer and Karlstrom, 2007]. The 1.4 Ga granitoids in the BRP and the Arizona Transition Zone represent the first major event to affect the Proterozoic lithosphere [Van Schmus et al., 1996], and were possibly produced from underplated basaltic material [Karlstrom and Humphreys, 1998].

[8] During the Mesozoic, the Laramide orogeny affected the southwestern United States with the arrival of a flat-lying subduction slab. Most of the current western U.S. orogenic zone including the study area was uplifted [Bird, 1979; Sonder and Jones, 1999]. During the subsequent tectonic collapse of the orogenic event in the Cenozoic, the current BRP area experienced widespread extension. The amount of extension in the BRP varied spatially, with the Colorado River Extensional Corridor being extended as much as 200% [Wernicke et al., 1988], leading to the formation of metamorphic core complexes (MCCs) which are exhumed metamorphic and igneous rocks in the previously over thickened crust [Coney and Harms, 1984]. At the present time, the southern BRP is characterized by low elevation, high heat flow [Lachenbruch and Sass, 1978], low upper mantle seismic velocities [Bensen et al., 2009; Buehler and Shearer, 2010], and thin crust [Zandt et al., 1995; Frassetto et al., 2006; Gilbert et al., 2007; Buehler and Shearer, 2010]. While the exact time of the uplift of the CP is still a topic of debate, most studies suggest that approximately during the same time period as the extension in the BRP, the CP was uplifted to about 2 km above sea level [Spencer, 1996; Sonder and Jones, 1999; Roy et al., 2009; Liu and Gurnis, 2010]. However, the interior of the CP remained unaffected by the extensional stress field.

[9] Central to this study is the nature and thickness of the crust under the CP and their relationship with the uplift and tectonic stability of the plateau. Despite the numerous studies on this fundamental problem, there still remains an uncertainty on the timing and the mechanism of the uplift of the CP, which was at or below sea level in the Late Cretaceous based on shallow marine deposits found

throughout the CP [Bond, 1976]. Paleobotanical [Wolfe et al., 1998], basalt vesicularity [Sahagian et al., 2002], and thermochronological studies [Flowers et al., 2008] resulted in contradictory data on the timing of the uplift, from the latest Cretaceous to the Miocene.

[10] Equally controversial is the mechanism for the uplift of the CP. Some of the proposed models include various crustal thickening models involving the flat subduction of the Farallon plate [Bird, 1984, 1988; Chase et al., 2002], thermal heating of the lithosphere [Hinojosa and Mickus, 2002], delimitation of a part or all of the mantle lithosphere [Bird, 1979; England and Houseman, 1988; Zandt et al., 1995; Spencer, 1996; McQuarrie and Chase, 2000], chemical alteration of the lithosphere and removal of the Farallon plate [Humphreys et al., 2003; Roy et al., 2004], mantle convection [Liu and Gurnis, 2010], and buoyancy from a lower velocity channel in the depth range of 150 to 300 km [West et al., 2004].

[11] Similarly, contradicting models for the thinning of the crust beneath the BRP have been proposed, including long-distance transportation of plastic lower crustal materials from the BRP to the CP [Bird, 1979, 1984], delamination of the lower crust, and Cenozoic extension [Wernicke et al., 1988] that created a radial anisotropy [Liu, 2009; Moschetti et al., 2010]. Isotopic [Livaccari and Perry, 1993] and xenolith [Esperanca et al., 1997; Selverstone et al., 1999] evidences indicate the presence of Proterozoic lower crust beneath the study area.

[12] The present study is aimed at providing constraints on the various models for the uplift and tectonic stability of the CP and crustal thinning of the BRP by systematically examining teleseismic receiver function data recorded at all the available broadband seismic stations in Arizona and adjacent areas. Gravity anomaly data are also used to aid in the interpretation of the seismic results and to provide additional constraints on the models.

3. Data and Methods

[13] The three-component broadband seismic data for all the seismic stations within the area of 31.5° to 37.0°N and -115.0° to -109.0°E were obtained from the IRIS (Incorporated Research Institutions for Seismology) DMC (Data Management Center). A total of 85 stations have available data at the IRIS DMC at the time when the data were requested. As described below, after the seismograms were

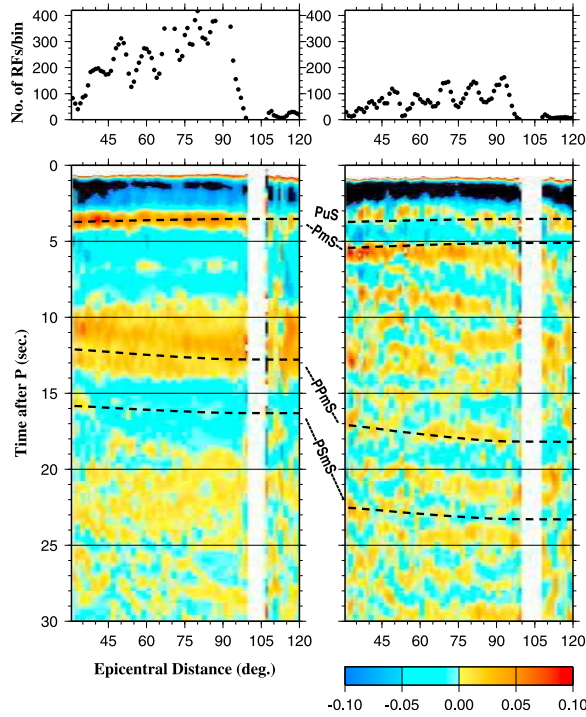


Figure 3. (bottom) Binned and stacked radial receiver functions from (left) stations in the BRP and (right) stations on the CP with observable PuS arrivals. Dashed lines are the predicted arrival times for PuS, PmS, PPmS, and PSmS phases. The scale bar shows the amplitude relative to that of the direct P wave. Note the clear difference in the arrival times of the converted phases and the existence of a midcrustal phase beneath the CP. (top) Number of RFs per bin.

converted into receiver functions and went through manual checking, 72 of them have sufficient high-quality RFs for the study. The 72 stations belong to a number of seismic networks including TA (EarthScope Transportable Array), IU (IRIS/USGS Network), CI (Caltech Regional Seismic Network), and several PASSCAL (Program for Array Seismic Studies of Continental Lithosphere) portable seismic networks. Sixty-four of the 72 stations (Figure 1) are TA stations which have a nominal spacing of 70 km and each station recorded the ground motion for about two years between 2007 and 2009. Station TUC belongs to the IU network, and stations NEE2, PDM, and GLA belong to the CI network. The data set also includes 4 stations from the LA RISTRA portable seismic experiment which recorded data for 18 months between August 1999 and May 2001 [Wilson et al., 2002].

[14] Data from earthquakes with epicentral distances between 30° and 180° for the period of 1990 to early 2010 were requested from the IRIS DMC for the study. Following Liu and Gao [2010], a

cutoff magnitude (M_c) was calculated using $M_c = 5.2 + (\Delta - 30.0)/(180.0 - 30.0) - D/700.0$, where Δ is the epicentral distance in degree, and D is the focal depth in km. The parameters used for this equation are aimed at balancing the quantity and quality of the seismic data to be requested.

[15] The seismograms were windowed starting 20 s before and extending to 360 s after the first P wave arrival, and were band-pass filtered within the frequency band of 0.08 to 0.8 Hz to improve signal-to-noise ratio (S/N). All the events having a S/N of 4.0 or greater on the radial component were selected and converted into radial RFs using the procedure of Ammon [1991]. The width of the Gaussian filter is 5 s, and the value of the water level is 0.03. The RFs were examined visually and all of those with well defined first P arrivals were selected for this study while the others with weak P arrivals or anomalously large peaks in the P wave coda were rejected. To ensure reliability of the results, 13 of the 85 stations with less than 40 high-quality RFs were not used in the study. A total of 15,766 high-quality RFs were used for the study at 72 stations, leading to an average of 219 RFs per station which is more than that used by most previous RF studies.

[16] To demonstrate the high-quality of the RFs and the first-order difference in crustal thickness between the BRP and the interior part of the CP, we grouped the RFs into (focal-depth corrected) epicentral distance bins of 2° wide and with 1° overlap among neighboring bins and stack those in the same bins (Figure 3). The arrival times of the PmS phase and its multiples for stations on the CP are significantly delayed relative to those on the BRP, suggesting a greater crustal thickness beneath the former.

[17] The resulting RFs for each of the stations were moveout-corrected and stacked [Zhu and Kanamori, 2000; Nair et al., 2006]. The optimal pair of crustal thickness (H) and V_p/V_s together with the maximum stacking amplitude (R) were determined for each station by grid searching. The stacking was performed using the equation [Zhu and Kanamori, 2000; Nair et al., 2006]

$$A(H_i, \phi_j) = \sum_{k=1}^n w_1 \times S_k(t_1^{(i,j)}) + w_2 \times S_k(t_2^{(i,j)}) - w_3 \times S_k(t_3^{(i,j)}), \quad (1)$$

where $\phi = V_p/V_s$, w_1 , w_2 , w_3 are the weighting factors, t_1 , t_2 , t_3 are the moveout times for the PmS, PPmS and PSmS phases, respectively, n is the

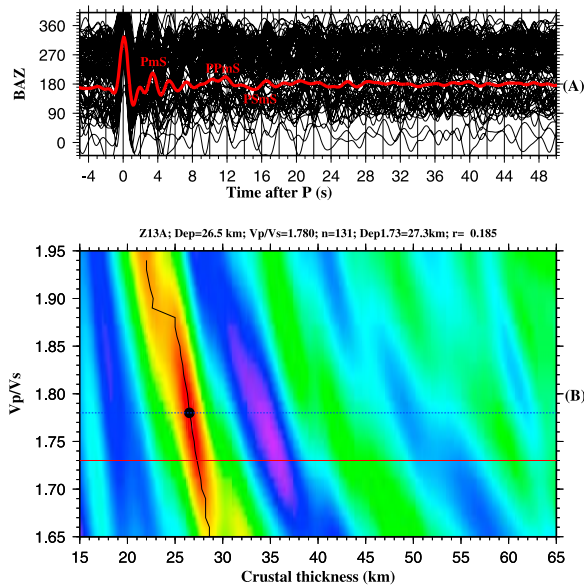


Figure 4. Analysis of data from station Z13A which is a quality A station located in central Arizona. (a) Radial receiver functions plotted against back-azimuth. The red line is the result of simple time domain stacking of all the RFs. *PmS* indicates *P*-to-*S* converted phases from the *Moho*, and *PPmS* and *PSmS* are multiples. (b) $H-\kappa$ plot. The black dot indicates the maximum stacking amplitude.

number of high-quality radial receiver functions from the station, $S_k(t)$ is the amplitude of the point on the k th receiver function at time t after the first *P* arrival, and $A(H_i, \phi_j)$ is the stacking amplitude corresponding to H_i and ϕ_j . For this study, we use $w_1 = 0.5$, $w_2 = 0.4$ and $w_3 = 0.1$. Figure 4 shows an example $H-\kappa$ (i.e., thickness versus V_p/V_s) plot and associated RFs.

[18] The procedure to produce the $H-\kappa$ plots involves calculation for a series of candidate H_i in the 15 to 65 km range with a 0.1 km increment, and ϕ_j values from 1.65 to 1.95 with a step of 0.0025. At each candidate (H_i, ϕ_j) , the RFs are stacked using Equation (1) to obtain $A(H_i, \phi_j)$. The effectiveness of the *Moho* in producing converted waves was quantified by R , which is the stacking amplitude (relative to that of the direct *P* wave) corresponding to the optimal H_i and ϕ_j . For each pair of (H_i, ϕ_j) , the moveout of *PmS*, *PPmS* and *PSmS*, were calculated. Details of stacking procedure including synthetic tests and the calculation of the moveout times can be found in the works of *Nair et al.* [2006] and *Liu and Gao* [2010].

[19] The computation of the moveout times requires a mean crustal *P* wave velocity. *Christensen and Mooney* [1995] found that the average crustal

velocity in crustal extensional domains is 6.2 km/s. Based on previous active and passive source seismic studies [*McCarthy et al.*, 1991; *Gish et al.*, 1981; *Frassetto et al.*, 2006], for this study, we used a crustal velocity of 6.1 km/s for the BRP and 6.3 km/s for the CP. As demonstrated by *Nair et al.* [2006], a 5% departure of the actual velocity from the velocity used for the stacking would lead to an error of about 2.5 km in the resulting H value, and about 0.012 in the resulting V_p/V_s value. The bootstrap approach was used to obtain the standard deviations (STDs) of the observed parameters (H , V_p/V_s , R) and their mean values [*Efron and Tibshirani*, 1986; *Press et al.*, 1996; *Gao et al.*, 2004; *Liu and Gao*, 2010].

[20] The Bouguer gravity anomaly data were obtained from the National Geospatial and Imaging Agency. The data set includes approximately 45,000 stations with the station spacing between 1 and 3 km except in the north central part of Arizona along the Utah border where the station spacing is greater 5 km. This distribution of data is sufficient for regional gravity studies and the construction of regional gravity models. In order to analyze lithospheric scale anomalies, an isostatic residual gravity anomaly map was created (Figure 5) using GMT (Generic Mapping Tools) software [*Wessel and Smith*, 1991] that uses the method of *Watts* [2001] to determine a regional compensation model where an elastic plate is flexed downward due to a driving load. The driving force is regional topographic loads as determined by elevations variations derived from GTOPO30 digital elevation models. Resulting isostatic residual gravity anomaly map (Figure 5) clearly outlines crustal scale features better than the Bouguer gravity anomaly map [*Sumner*, 1989; *Hendricks and Plescia*, 1991]. The Bouguer gravity anomaly map shows a large amplitude northeast trending gradient that is related to the change in crustal thickness between the CP and the BRP. The isostatic residual gravity anomaly map still has northeast trending gradient but its amplitude is less than half of that on the Bouguer gravity anomaly map. The high amplitude regions which are more pronounced in the isostatic residual gravity anomaly map in southwest Arizona and along the Colorado River can be explained by high density lower crustal material as imaged by seismic refraction surveys [*McCarthy et al.*, 1991].

4. Results

[21] Reliable crustal thickness (Figure 5), V_p/V_s (Figure 6), and amplitude ratio (Figure 7) observa-

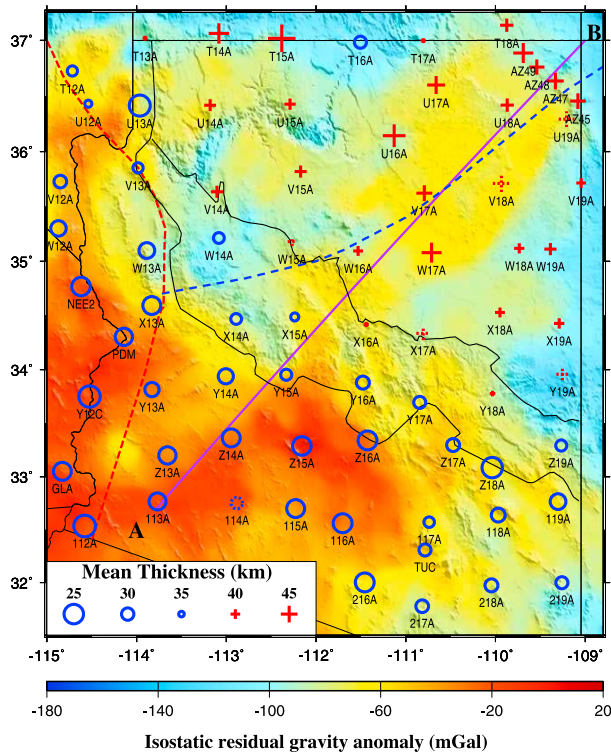


Figure 5. Resulting crustal thicknesses plotted on top of isostatic residual gravity anomaly map. Pluses indicate the stations with a large thickness, and open circles indicate relatively smaller thicknesses (see legend). Solid symbols represent category A stations, and dotted ones represent category B stations. Line A-B is the location of the gravity model shown in Figure 9.

tions were obtained at 72 stations. We divide the results into two categories (A and B) based on the quality of the RFs (Table 1). Stations in category A display a clear PmS arrival between 3.5 and 6.5 s and either a $PPmS$ or $PSmS$ or both arrivals, leading to a well-defined single peak on the $H - \kappa$ plot (see Figure 4 for an example). Those in category B show a clear PmS arrival but neither $PPmS$ nor $PSmS$ is observed, resulting in a poorly defined peak on the $H - \kappa$ plot (see Nair *et al.* [2006] for results of synthetic tests). For category B stations V_p/V_s cannot be reliably determined, and the crustal thickness is taken as H_n which is the thickness corresponding to a nominal V_p/V_s of 1.732. Fortunately, the vast majority (66 out of 72) of the stations turned out to be category A stations, and the remainder are category B stations.

[22] The resulting V_p/V_s values of all 66 stations for the PmS arrival in the entire study area range from 1.64 to 1.97 with an average of 1.797 ± 0.008 , H values range from 23 km to 54 km with a mean

value of 34.4 ± 0.9 km, and the resulting R values range from 0.05 to 0.36 with a mean of 0.155 ± 0.008 . To highlight systematic spatial variations of the observed crustal characteristics, we plot elevation and the H , V_p/V_s , and R values observed in a 200 km wide NE-striking band (Figure 8). The observed crustal parameters correspond well with surface elevation. Based on seismically derived crustal characteristics, tectonic history and surface geology, we divide the study area into five subareas (Figure 1). As detailed below, our results are in excellent agreement with the vast majority of results from previous studies. One exception is that at some stations, our results are inconsistent with those from EARS (the EarthScope Automated Receiver Survey, <http://www.iris.edu/dms/products/ears/>). The disagreement is most likely caused by the fact that the automatic procedure includes low-quality RFs, while our and most other previous studies performed manual checking of the RFs before they were used for stacking.

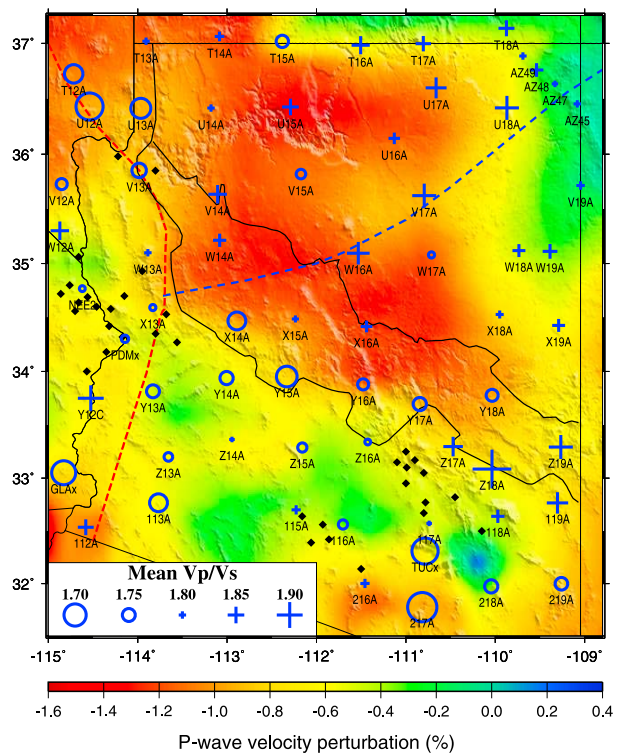


Figure 6. Resulting crustal V_p/V_s derived from category A stations. The background image shows P wave velocity perturbations relative to the AK135 earth model [Kennett *et al.*, 1995] at the depth of 100 km [Burdick *et al.*, 2010]. Pluses indicate relatively larger values, and circles indicate relatively smaller values (see legend). The black diamonds indicate the locations of diabase sheeted intrusions [Howard, 1991; Karlstrom and Humphreys, 1998].

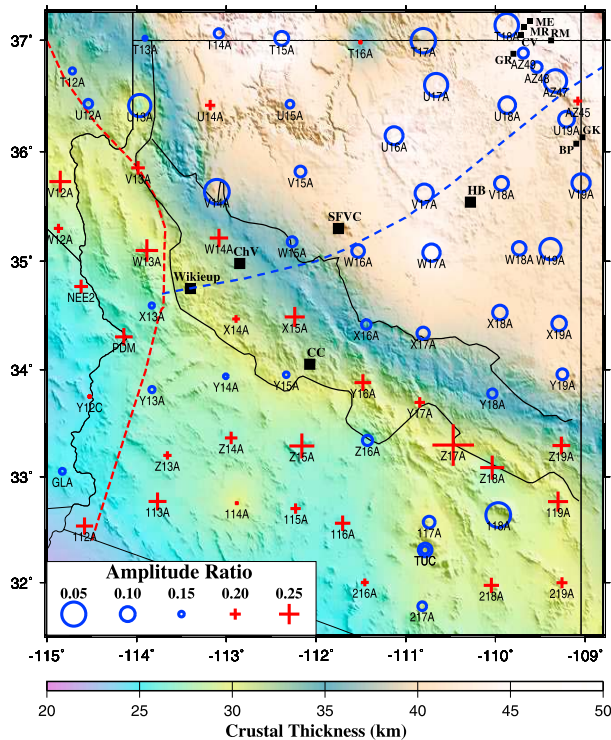


Figure 7. Observed amplitude ratio (R) plotted on top of smoothed crustal thickness measurements shown in Figure 5. The dashed lines are terrane boundaries (see Figure 1). The black squares indicate the locations for xenolith data [Selverstone *et al.*, 1999; McGuire, 1994]. CC, Cache Creek; ChV, Chino Valley; SFVC, San Francisco volcanic field; HB, Hopi Buttes; BP, Buell Parks; GK, Green Knobs; GR, Garnet Ridge; CV, Cane Valley; MR, Moses Rock; RM, Red Mesa; ME, Muler Ear.

4.1. Area A

[23] Area A, which contains 4 stations, is a transition zone between the northwestern CP and the adjacent BRP [Wooden and DeWitt, 1991] (Figure 1). The resulting crustal thickness ranges from 24 to 35 km in the BRP to 40 km at the western edge of the CP (Figure 5). The thinnest crust occurs over a large Cenozoic volcanic field (Figure 1). These observations agree well with the isostatic residual gravity anomaly patterns (Figure 5) which show gravity maxima over the extended and thin crust in the BRP [Mickus and James, 1991] and a gravity minimum over the thick crust.

[24] The average crustal thickness beneath this area is 31.5 ± 2.7 km with a mean V_p/V_s value of 1.726 ± 0.026 which is the smallest values of entire study area. In addition, the R value (0.125 ± 0.022) is smaller than the mean value (0.155 ± 0.008) in the entire study area. By stacking RFs recorded at

7 stations in this area, Zandt *et al.* [1995] reported that the crustal thickness ranges from 30 to 35 km with an average V_p/V_s of 1.73 (Figure 2), values consistent with our measurements.

4.2. Area B

[25] Area B is within the Colorado River Extensional Corridor of the BRP, a region of highly extended crust [Howard and John, 1987; Mickus and James, 1991]. Analysis of data from the ten stations in this area resulted in crustal thicknesses ranging from 23 to 32 km (Figure 5), which is among the thinnest in the entire study area. This agrees with seismic refraction [McCarthy *et al.*, 1991] and gravity modeling results [Mickus and James, 1991]. The mean V_p/V_s (1.795 ± 0.019) value is close to the mean value of the entire study area, and the mean R value (0.207 ± 0.013) is significantly greater than the mean value of the study area.

[26] Zhu and Kanamori [2000] measured H and V_p/V_s at two stations (GLA and NEE) in area B. At station GLA, our resulting crustal thickness (26.1 ± 0.4 km) and V_p/V_s (1.70 ± 0.20) values are consistent with the results of Zhu and Kanamori [2000] (27.0 ± 0.6 km and 1.72 ± 0.04 , respectively). Another station measured by Zhu and Kanamori [2000], NEE, is about 6.5 km north of our station NEE2. The resulting crustal thicknesses are similar (31.3 ± 1.3 km for NEE and 25.7 ± 0.2 km for NEE2), and the V_p/V_s values are statistically consistent (1.75 ± 0.05 versus 1.79 ± 0.01).

4.3. Area C

[27] Area C is within the BRP of southern Arizona and contains 17 stations. The resulting crustal thicknesses range from 25 to 33 km with an average of 28.2 ± 0.5 km (Figure 5), V_p/V_s values range from 1.65 to 1.86 with an average of 1.761 ± 0.014 (Figure 6), and R values from 0.05 to 0.28 with an average of 0.181 ± 0.014 (Figure 7).

[28] Within this area, the crust is thinner (25–28 km compared to 30–33 km) in western Arizona than southeastern Arizona. This relationship can also be observed in the isostatic residual gravity anomaly where higher amplitude regional gravity anomalies are seen in western Arizona than in southeastern Arizona (Figure 5). Additionally, although areas B and C are usually considered as a single tectonic unit (southern Basin and Range), there are enough contrasts in V_p/V_s , and R values between the two areas to indicate that the crust may have different

Table 1. Observations of Crustal Thickness (H , H_n), V_p/V_s (ϕ), and R

Station	Area	Longitude (deg),	Latitude (deg)	H (km)	ϕ	H_n (km)	R	N	Rank
112A	B	-114.580	32.536	23.5 ± 0.28	1.846 ± 0.015	25.4 ± 0.13	0.233 ± 0.007	136	A
113A	C	-113.767	32.768	26.9 ± 0.18	1.724 ± 0.005	26.7 ± 0.04	0.237 ± 0.015	196	A
114A	C	-112.883	32.751	–	–	30.9 ± 0.15	0.162 ± 0.004	122	B
115A	C	-112.228	32.701	26.0 ± 0.00	1.810 ± 0.000	27.1 ± 0.07	0.196 ± 0.006	243	A
116A	C	-111.704	32.562	25.5 ± 0.17	1.770 ± 0.005	26.2 ± 0.09	0.223 ± 0.003	274	A
117A	C	-110.739	32.572	31.5 ± 0.00	1.790 ± 0.000	32.3 ± 0.00	0.117 ± 0.005	177	A
118A	C	-109.970	32.640	29.0 ± 0.33	1.832 ± 0.013	30.7 ± 0.22	0.047 ± 0.006	46	A
119A	C	-109.303	32.766	27.6 ± 0.20	1.876 ± 0.005	30.0 ± 0.05	0.249 ± 0.003	199	A
216A	C	-111.457	32.002	25.4 ± 0.16	1.810 ± 0.010	26.7 ± 0.04	0.182 ± 0.006	192	A
217A	C	-110.816	31.775	30.0 ± 0.09	1.662 ± 0.004	28.8 ± 0.13	0.134 ± 0.006	199	A
218A	C	-110.046	31.974	29.6 ± 0.09	1.748 ± 0.004	30.0 ± 0.00	0.223 ± 0.003	228	A
219A	C	-109.259	31.999	30.4 ± 0.00	1.752 ± 0.004	30.8 ± 0.00	0.199 ± 0.004	176	A
AZ45	E	-109.082	36.455	44.2 ± 0.00	1.800 ± 0.000	50.1 ± 0.12	0.188 ± 0.012	103	A
AZ47	E	-109.333	36.636	45.0 ± 0.07	1.795 ± 0.007	47.9 ± 2.83	0.058 ± 0.005	146	A
AZ48	E	-109.539	36.761	44.0 ± 0.61	1.834 ± 0.025	47.6 ± 2.86	0.123 ± 0.017	95	A
AZ49	E	-109.691	36.887	47.5 ± 0.10	1.800 ± 0.000	49.7 ± 0.00	0.124 ± 0.005	164	A
GLA	B	-114.827	33.051	26.1 ± 0.35	1.690 ± 0.020	25.5 ± 0.05	0.148 ± 0.015	39	A
NEE2	B	-114.619	34.768	25.7 ± 0.13	1.788 ± 0.011	26.7 ± 0.00	0.214 ± 0.006	320	A
PDM	B	-114.142	34.303	26.5 ± 0.00	1.780 ± 0.000	27.5 ± 0.00	0.235 ± 0.003	465	A
T12A	A	-114.715	36.726	31.7 ± 0.05	1.720 ± 0.000	31.6 ± 0.00	0.146 ± 0.007	191	A
T13A	A	-113.907	37.020	36.5 ± 0.00	1.800 ± 0.000	38.0 ± 0.05	0.159 ± 0.013	205	A
T14A	E	-113.084	37.062	47.7 ± 0.09	1.812 ± 0.004	52.5 ± 0.05	0.129 ± 0.005	225	A
T15A	E	-112.382	37.018	52.8 ± 0.13	1.753 ± 0.005	53.5 ± 0.24	0.104 ± 0.006	204	A
T16A	E	-111.506	36.984	30.4 ± 0.32	1.858 ± 0.013	33.2 ± 0.22	0.165 ± 0.012	128	A
T17A	E	-110.804	36.997	36.6 ± 0.35	1.844 ± 0.006	39.5 ± 0.15	0.048 ± 0.004	180	A
T18A	E	-109.874	37.136	42.5 ± 0.29	1.847 ± 0.012	44.9 ± 0.00	0.053 ± 0.003	236	A
TUC	C	-110.785	32.310	30.3 ± 0.04	1.678 ± 0.004	29.6 ± 0.19	0.138 ± 0.009	272	A
U12A	A	-114.539	36.432	33.8 ± 0.13	1.674 ± 0.000	0.0 ± 0.00	0.133 ± 0.007	254	A
U13A	A	-113.965	36.415	23.8 ± 0.39	1.711 ± 0.017	0.0 ± 0.00	0.060 ± 0.010	140	A
U14A	E	-113.180	36.418	41.5 ± 0.05	1.800 ± 0.000	43.2 ± 0.09	0.196 ± 0.004	219	A
U15A	E	-112.291	36.428	41.1 ± 0.00	1.850 ± 0.000	47.6 ± 0.22	0.139 ± 0.003	197	A
U16A	E	-111.130	36.143	49.3 ± 0.10	1.822 ± 0.005	51.6 ± 0.00	0.084 ± 0.003	197	A
U17A	E	-110.662	36.600	45.9 ± 0.15	1.873 ± 0.006	53.1 ± 0.23	0.056 ± 0.003	253	A
U18A	E	-109.870	36.420	42.6 ± 0.07	1.890 ± 0.000	44.0 ± 9.33	0.090 ± 0.013	166	A
U19A	E	-109.208	36.292	–	–	44.3 ± 0.07	0.095 ± 0.004	124	B
V12A	B	-114.851	35.727	29.9 ± 0.00	1.760 ± 0.000	30.4 ± 0.07	0.258 ± 0.005	244	A
V13A	B	-113.984	35.852	31.6 ± 0.00	1.742 ± 0.004	32.0 ± 0.00	0.214 ± 0.008	182	A
V14A	E	-113.105	35.634	41.8 ± 0.85	1.860 ± 0.028	46.9 ± 2.83	0.047 ± 0.002	243	A
V15A	E	-112.173	35.819	41.7 ± 0.13	1.768 ± 0.004	42.8 ± 0.04	0.121 ± 0.004	234	A
V17A	E	-110.794	35.622	44.4 ± 0.31	1.890 ± 0.000	55.0 ± 1.62	0.082 ± 0.002	114	A
V18A	E	-109.933	35.711	–	–	45.4 ± 4.39	0.105 ± 0.007	109	B
V19A	E	-109.046	35.715	40.0 ± 0.24	1.806 ± 0.009	44.1 ± 0.00	0.082 ± 0.002	240	A
W12A	B	-114.870	35.301	27.8 ± 0.00	1.860 ± 0.000	32.4 ± 0.00	0.190 ± 0.005	315	A
W13A	B	-113.885	35.099	27.7 ± 0.00	1.800 ± 0.000	28.7 ± 0.00	0.262 ± 0.003	340	A
W14A	D	-113.083	35.213	31.3 ± 0.22	1.832 ± 0.008	33.4 ± 0.18	0.239 ± 0.004	330	A
W15A	E	-112.267	35.179	–	–	39.4 ± 0.00	0.127 ± 0.003	290	B
W16A	E	-111.532	35.095	40.1 ± 0.10	1.883 ± 0.010	47.2 ± 2.96	0.111 ± 0.007	195	A
W17A	E	-110.713	35.079	47.3 ± 0.17	1.787 ± 0.006	48.6 ± 0.00	0.086 ± 0.002	230	A
W18A	E	-109.736	35.118	40.3 ± 0.00	1.830 ± 0.000	38.1 ± 11.98	0.107 ± 0.008	288	A
W19A	E	-109.388	35.112	41.8 ± 0.05	1.840 ± 0.000	44.1 ± 0.04	0.066 ± 0.004	250	A
X13A	B	-113.830	34.593	26.0 ± 0.15	1.786 ± 0.009	26.8 ± 0.05	0.152 ± 0.004	303	A
X14A	D	-112.891	34.469	31.2 ± 0.10	1.722 ± 0.005	31.1 ± 0.00	0.182 ± 0.003	353	A
X15A	D	-112.237	34.487	33.2 ± 0.09	1.798 ± 0.004	34.7 ± 0.04	0.248 ± 0.002	299	A
X16A	E	-111.441	34.418	36.7 ± 0.21	1.823 ± 0.015	38.2 ± 0.26	0.129 ± 0.002	229	A
X17A	E	-110.806	34.337	–	–	42.9 ± 0.00	0.113 ± 0.007	181	B
X18A	E	-109.950	34.529	40.2 ± 0.06	1.803 ± 0.006	41.9 ± 0.00	0.101 ± 0.005	265	A
X19A	E	-109.290	34.428	40.4 ± 0.21	1.830 ± 0.008	46.5 ± 0.06	0.101 ± 0.002	259	A
Y12C	B	-114.524	33.750	23.7 ± 0.00	1.900 ± 0.000	30.9 ± 0.11	0.167 ± 0.003	441	A
Y13A	C	-113.829	33.814	28.8 ± 0.00	1.750 ± 0.000	29.0 ± 0.21	0.146 ± 0.001	360	A
Y14A	C	-113.005	33.938	28.1 ± 0.13	1.748 ± 0.004	28.3 ± 0.00	0.156 ± 0.004	346	A
Y15A	D	-112.333	33.953	31.0 ± 0.22	1.708 ± 0.011	30.7 ± 0.09	0.151 ± 0.004	212	A

Table 1. (continued)

Station	Area	Longitude (deg),	Latitude (deg)	H (km)	ϕ	H_n (km)	R	N	Rank
Y16A	D	-111.478	33.880	29.6 ± 0.04	1.760 ± 0.000	30.2 ± 0.09	0.230 ± 0.005	244	A
Y17A	D	-110.844	33.695	30.4 ± 0.00	1.748 ± 0.004	30.8 ± 0.00	0.197 ± 0.007	195	A
Y18A	D	-110.034	33.778	37.0 ± 0.06	1.755 ± 0.006	37.4 ± 0.13	0.130 ± 0.009	220	A
Y19A	E	-109.254	33.957	–	–	41.7 ± 0.00	0.121 ± 0.008	190	B
Z13A	C	-113.657	33.200	26.6 ± 0.16	1.774 ± 0.009	27.4 ± 0.11	0.185 ± 0.006	131	A
Z14A	C	-112.946	33.363	26.0 ± 0.00	1.790 ± 0.000	27.1 ± 0.00	0.208 ± 0.005	407	A
Z15A	C	-112.158	33.289	25.7 ± 0.00	1.770 ± 0.000	26.3 ± 0.00	0.275 ± 0.003	235	A
Z16A	D	-111.427	33.341	25.4 ± 0.21	1.788 ± 0.011	26.3 ± 0.00	0.125 ± 0.005	243	A
Z17A	D	-110.472	33.297	29.8 ± 0.17	1.866 ± 0.009	36.3 ± 2.41	0.364 ± 0.007	88	A
Z18A	D	-110.036	33.085	24.4 ± 0.00	1.970 ± 0.000	27.9 ± 0.00	0.270 ± 0.006	103	A
Z19A	D	-109.266	33.292	31.0 ± 0.08	1.890 ± 0.000	34.6 ± 1.52	0.236 ± 0.007	147	A

characteristics. This might be reflected in the degrees of extension between the two areas and the presence of a lower crustal domal region in the Colorado River Extensional Corridor [Mickus and James, 1991; McCarthy et al., 1991].

[29] Frassetto et al. [2006] analyzed RFs at COARSE (Consortium for an Arizona Reconnaissance Seismic Experiment) stations and concluded that the average crustal thickness in the BRP in Arizona is about 28 km, which is consistent with our results. The mean value of V_p/V_s obtained by Frassetto et al. [2006] in the BRP is 1.78 which is similar to our result of 1.761 ± 0.014 for area C. Our crustal thickness measurements in this area are in agreement with results obtained by Gilbert et al. [2007] using RF stacking, and with results from seismic refraction data [Parsons et al., 1996; Gish et al., 1981; Sinno et al., 1981; Warren, 1969] (Figure 2).

4.4. Area D

[30] Area D has 11 stations within the Arizona Transition Zone. The resulting crustal thicknesses range from 25 to 33 km, V_p/V_s values range from 1.65 to 1.88, and R measurements range from 0.05 to 0.28. The corresponding averages are 30.4 ± 1.0 km, 1.803 ± 0.024 , and 0.216 ± 0.021 for H , V_p/V_s , and R measurements, respectively.

[31] Gish et al. [1981] modeled seismic refraction data and concluded that the crustal thickness beneath the Arizona Transition Zone is about 32 km which is slightly larger than our results. Frassetto et al. [2006] concluded that beneath station RENO, which is located in the southeastern part of Transition Zone, the crustal thickness ranges from 34.5 to 36.5 km and V_p/V_s ranges from 1.81 to 1.86 which are consistent with the results from a nearby station (Z19A) in this study (Table 1).

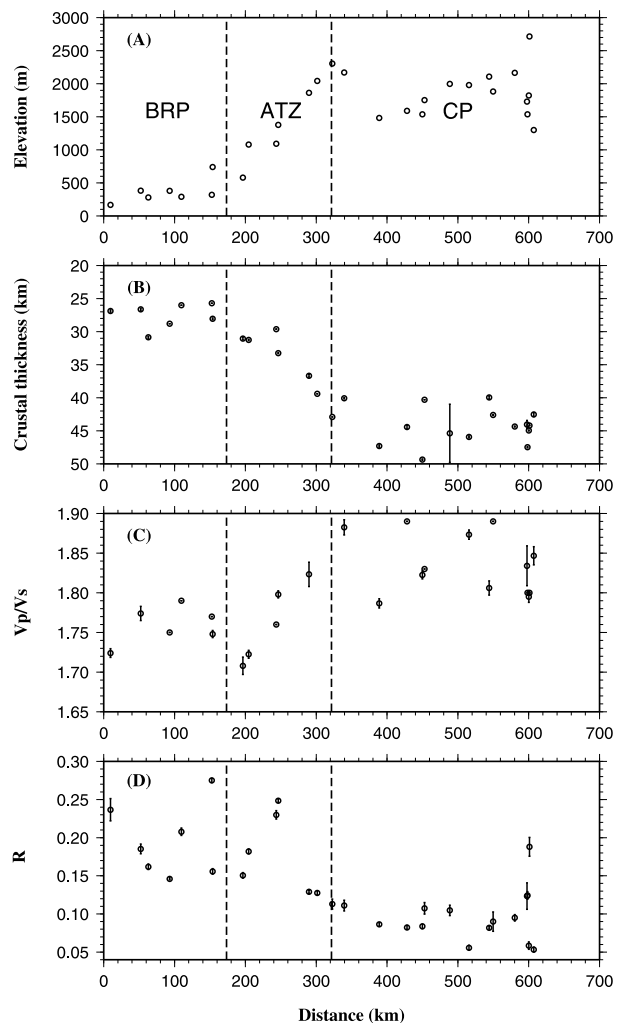


Figure 8. Cross-section plots for (a) elevation, (b) H , (c) V_p/V_s , and (d) R observations at stations in a 200 km wide band centered at profile A-B shown in Figure 5. BRP, Basin and Range Province; ATZ, Arizona Transition Zone; CP, Colorado Plateau.

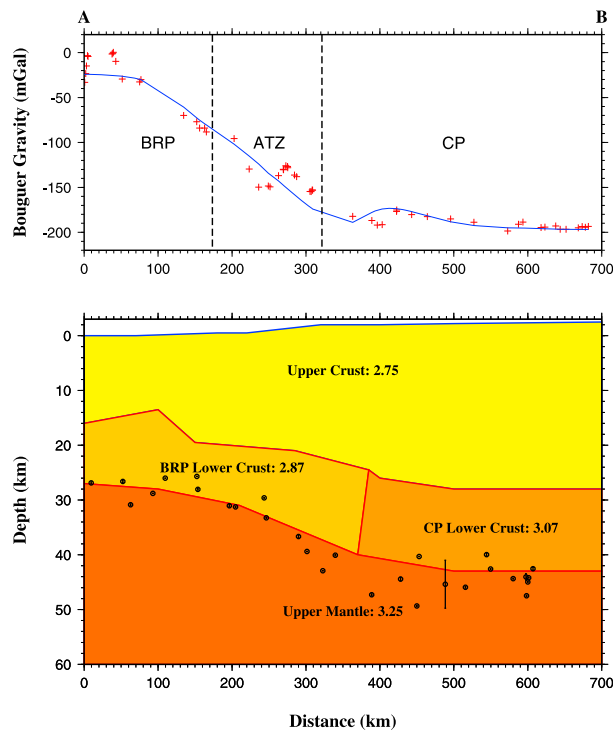


Figure 9. Gravity model of the crust and upper mantle along profile A-B (Figure 5). Densities are in g/cm^3 . The red crosses are observed and the blue line is calculated gravity anomalies. Dots represent crustal thickness determinations at stations in the 200 km wide band centered on the profile.

Gilbert et al. [2007], *McCarthy et al.* [1994], and *Warren* [1969] suggested that crustal thickness beneath the Transition Zone ranges from 30 to 35 km (Figure 2), which agrees with our results.

4.5. Area E

[32] Area E is the SW portion of the CP and contains the maximum number of stations (30) among all the five areas. The resulting H measurements range from 30 to 53 km with a mean value of 42.3 ± 0.79 km, which is the largest among all the five areas. Similarly, the V_p/V_s measurements range from 1.65 to 1.89 with a mean value of 1.825 ± 0.009 , which is also the largest among all the areas. In contrast, the R values range from 0.048 to 0.196 with a mean of 0.105 ± 0.007 , which is the lowest in the entire study area.

[33] Our results are consistent with most of the previous determinations of crustal characteristics. Seismic refraction experiments revealed a crust with a thickness ranging from 40 to 45 km [*Roller*, 1965; *Warren*, 1969; *Prodehl*, 1979; *Wolf and Cipar*, 1993; *Parsons et al.*, 1996]. *Hauser and*

Lundy [1989] combined COCORP reflection data with results previously obtained by *Roller* [1965] and *Warren* [1969], and suggested that the minimum crustal thickness of the CP is 50 km (Figure 2). *Zandt et al.* [1995] used the receiver function technique at 11 seismic stations along $37^\circ N$ latitude and proposed that the average crustal thickness and the V_p/V_s beneath the western CP is 45 km and 1.85, respectively. *Frassetto et al.* [2006] stacked receiver functions at COARSE seismic stations and concluded that the average crustal thickness and the V_p/V_s beneath the southern part of the CP is 40 km and 1.81, respectively. Using data from COARSE and LA RISTRA, *Gilbert et al.* [2007] suggested that the crustal thickness ranges from 35 to 45 km with V_p/V_s values in the range of 1.81–1.85. *Sheehan et al.* [1997] used the receiver function technique and proposed that the average crustal thickness beneath the northeastern part of the CP is 43.1 km. Those observations are in general agreement with our results.

4.6. Gravity Modeling

[34] The isostatic residual gravity anomaly map (Figure 5) highlights the relationships between the gravity field, resulting crustal thickness, and the tectonic regimes. Gravity anomalies and crustal thickness relationships have been discussed by previous researchers [e.g., *Aiken*, 1976; *Sumner*, 1989; *Hendricks and Plescia*, 1991]. In general, areas with thicker crust are characterized by more negative isostatic gravity anomalies and vice versa. In order to aid in determining if the above crustal thicknesses agree with other geophysical data, a two and one-half dimensional gravity model using the method of *Cady* [1980] was constructed using the observed Bouguer gravity anomaly data. The elevation of the data points and surface topographic variations were used in the modeling process. A variety of constraints were used to construct the final model (Figure 9) including receiver function derived crustal thicknesses (Figure 8), seismic refraction models [*Warren*, 1969; *Wolf and Cipar*, 1993; *McCarthy et al.*, 1991], and P wave velocities converted to densities [*Christensen and Mooney*, 1995]. The densities derived from the P wave velocities and the seismically derived thicknesses were altered by up to 10% to determine a final gravity model.

[35] The resulting gravity model (Figure 9) shows a 12–15 km thick high-density lower crustal layer beneath the CP, supporting the existence of the lower crustal layer between the *Moho* and the

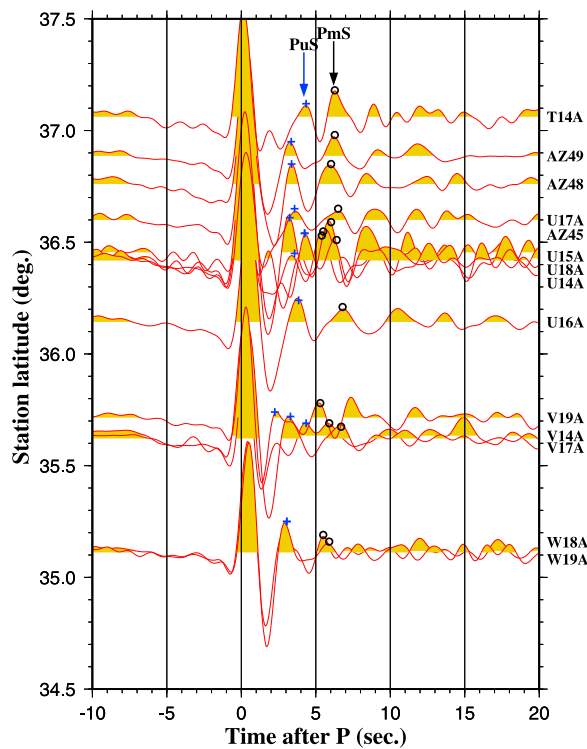


Figure 10. Stacked RFs for stations with observable *PuS* arrivals plotted against station latitudes. The *PuS* arrivals are marked by crosses, and the *PmS* are marked by circles.

crustal discontinuity responsible for generating the observed *PuS* (Figure 10, see below). In addition, the gravity model requires that the density of the lower crust beneath the CP must be significantly greater than that beneath the BRP. The resulting lower crustal densities are 2.87 g/cm^3 for the BRP and 3.07 g/cm^3 for the CP, which is about 5% higher than the lower crustal density in the IASP91 earth model [Kennett and Engdahl, 1991]. This implies the existence of a mafic lower crustal layer beneath the CP, a conclusion that is consistent with the distribution of the V_p/V_s observations (Figures 6 and 8).

5. Discussion

5.1. Crustal Composition

[36] Crustal composition for the study area can be determined with the help of our geophysically derived crustal parameters. Christensen [1996] made laboratory measurements and concluded that the average V_p/V_s value of upper and lower continental crust is about 1.74 and 1.81, respectively, leading to an average value of 1.78 for the entire continental crust. Additionally, Holbrook

et al. [1992] concluded that V_p/V_s values smaller or equal to 1.76 are indicative of felsic rocks, 1.78 to 1.81 are intermediate, and ≥ 1.81 are associated with mafic rocks. Based on the above criteria, the overall crustal composition is felsic for area A, intermediate for areas B, C, and D, but approaches mafic for area E. This can be seen in the gravity model in which the CP has an overall denser crust than the BRP. The densities of the lower crust is 3.07 g/cm^3 for the CP and 2.87 g/cm^3 for the BRP which is consistent with mafic and intermediate petrologies, respectively.

[37] Areas B and C are both in extensional terranes of the BRP but the V_p/V_s values of the former (1.795 ± 0.019) are considerably larger than those of the latter (1.761 ± 0.014 , see Figure 6). The difference might be related to the presence of more abundant gabbroid diabase sheets, which have a high V_p/V_s , in area B than that in area C (Figure 6) [Howard, 1991; Karlstrom and Humphreys, 1998]. Alternatively, the larger V_p/V_s in area B can be caused by a previously proposed lower crustal domal structure seen in the seismic refraction and gravity models [McCarthy *et al.*, 1991; Mickus and James, 1991]. This structure would cause the overall densities and V_p/V_s to be higher than those observed in area C.

5.2. Constraints on Hypotheses of Crust Thinning Beneath the BRP

[38] Several models have been proposed to explain the significantly thinned crust beneath the BRP. In light of our new RF measurements, we next provide new constraints on these models.

5.2.1. Mesozoic Compression and Transportation of Lower Crustal Material Beneath the BRP

[39] A number of studies have proposed that a layer of the lower crust was transported from the BRP toward the CP due to Mesozoic compression associated with the flat-subduction of the Farallon plate [Bird, 1979, 1984, 1988; Zandt *et al.*, 1995], resulting in a thinned BRP and thickened CP crust. This model predicts that relative to a typical continental cratonic area, the BRP should have reduced crustal thickness (H) and V_p/V_s observations due to the removal of a mafic lower crustal layer, and perhaps increased R values due to an increase in the velocity contrast between the mantle and the overlying upper crust.

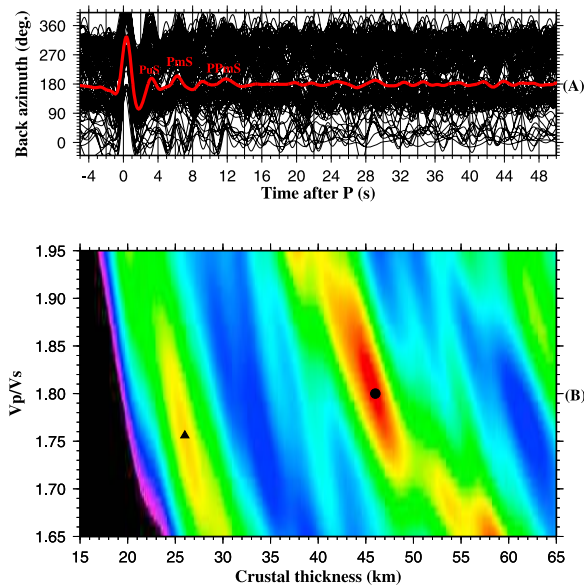


Figure 11. (a) Individual (thin black lines) and stacked (thick red line) receiver functions for station AZ49, showing the PuS arrival at about 3 s after the direct P wave. (b) Corresponding $H - \kappa$ plot. The dot in Figure 11b corresponds to the optimal H and V_p/V_s associated with the *Moho*, and the triangle represents the optimal values for the boundary at the top of the lower crustal layer.

[40] While this model can explain the observed thin crust, the anticipated decrease in V_p/V_s and increase in R are not observed (Figures 6 and 7). Instead, the mean V_p/V_s over the southern BRP stations (areas B and C) is 1.773 ± 0.012 which is almost identical to the V_p/V_s of a typical continental crust (1.78) [Christensen, 1996] that contains both the upper and lower crust. In addition, the observed R values are similar to typical continental cratons such as the undeformed part of the Kaapvaal craton in southern Africa [Nair *et al.*, 2006]. Therefore, the long distance transportation of lower crust material away from the BRP is inconsistent with our observations.

5.2.2. Delamination of the Lower Crust Beneath the BRP

[41] The thin crust, high heat flow, and high isostatic residual gravity anomalies (Figure 5) in the BRP area might suggest that the lower crust beneath the BRP has been removed by delamination [Gao *et al.*, 1998; Jull and Kelemen, 2001]. Crustal delamination can occur in continental regions which are going through extension such as the BRP [Jull and Kelemen, 2001; Gans and Bohrsen, 1998]. The loss of the lower crust to the mantle would lead to an overall felsic crust and an increase in R due

to direct contact between the subcrustal lithosphere and the upper crust. Both are not observed at the BRP stations (Figures 6 and 7), suggesting that our observations are not supportive of lower crustal delamination beneath the BRP. This conclusion is consistent with results from Nd isotopic studies which indicate that a 70 to 100 km thick lithosphere existed beneath both the BRP and the CP between early Proterozoic and late Cenozoic time [Livaccari and Perry, 1993]. A post-Proterozoic crustal delamination event would require the removal of the original lithosphere and consequent formation of a younger lithosphere.

5.2.3. Cenozoic Extension in the BRP

[42] Numerous studies suggest that the BRP has been extended by as much as 200% during the middle to late Cenozoic [Gans and Bohrsen, 1998; Wernicke *et al.*, 1988]. Under the assumption of a 100% extension rate, our observed present-day crustal thickness (23–32 km) in the BRP suggests a pre-Cenozoic crustal thickness of about 50 km, which is similar to the value that Zandt *et al.* [1995] proposed in the NW corner of the study area (Figure 2).

[43] Our observations of small H , normal V_p/V_s and normal R values (relative to a typical cratonic area) in the BRP are consistent with the model that the thinned crust beneath the BRP was the consequence of significant Cenozoic extension, because a simple extension of both the upper and lower crust reduces the crustal thickness but maintains the preextension V_p/V_s and R values.

5.3. A Strong Mafic Lower Crustal Layer Beneath the CP

[44] A total of 14 stations show a clear arrival prior to PmS which is denoted as PuS (Figures 3 and 10). The arrival and associated multiples result in a clearly defined secondary peak on the $H - \kappa$ plot (see Figure 11 for an example). All of the stations with the PuS arrival are located on the CP (Figure 1). We determined the values of H , V_p/V_s and R related to the PuS arrival using the same $H - \kappa$ stacking procedure used to determine the parameters for the entire crust. The resulting thicknesses of the upper crustal range from 26.2 to 35.9 km with a mean of 30.1 ± 0.9 km, and the V_p/V_s values range from 1.66 to 1.79 with a mean of 1.734 ± 0.011 , which are significantly smaller than those for the entire crust and are consistent with laboratory-determined V_p/V_s of upper continental crust rocks [Christensen, 1996]. The R measurements associated with the PuS

arrival range from 0.012 to 0.177 with a mean of 0.095 ± 0.011 . Although *PuS* arrivals are not as clearly observed at the rest of the CP stations, probably due to a less sharp discontinuity, the similarities in the H , V_p/V_s , and R observations (Figures 5–7) between the stations with and without the *PuS* arrival indicate a stratified crustal structure beneath the CP.

[45] Given the observed mean H of 42 km and a mean V_p/V_s of 1.825 for the entire CP crust, we can estimate the V_p/V_s of the 12 km thick lower crustal layer by simple partitioning, i.e., $H_U\phi_U + H_L\phi_L = H\phi$, where $\phi = V_p/V_s = 1.825$, $H = 42.0$ km, $\phi_U = 1.734$, $H_U = 30.0$ km, and $H_L = 12$ km. The resulting V_p/V_s for the lower layer, ϕ_L , is 2.053, which is about 13% greater than that of typical lower crustal rocks [Christensen, 1996], suggesting a composition with more Fe and Mg than a typical lower crustal layer.

[46] The existence of the mafic layer beneath the CP is supported by results of gravity modeling (Figure 9), which suggest that the lower crust under the CP has a higher density than that beneath the BRP. Of course, the exact density could not be determined based on gravity modeling alone due to trade-offs between the thickness and density of the layers in the model, but a density greater than 3.00 g/cm³ had to be used for the CP lower crust in order to match the observed anomalies. Such densities are consistent with mafic rocks [e.g., Christensen, 1996].

[47] This strongly mafic lower crustal layer increases the overall crustal V_p/V_s , as observed (Figure 6), and reduces the velocity contrast across the *Moho*, leading to the observed anomalously small R observations on the CP (Figure 7). In turn, the fact that almost all the CP stations show large H , large V_p/V_s , and small R observations strongly suggest that the lower crustal layer pervasively exists beneath the entire CP interior and is not limited to stations with clear *PuS* arrivals.

[48] Seismic refraction/wide-angle reflection data obtained along most of the PACE (Pacific to Arizona Crustal Experiment) profiles across the CP (Figure 2) show a high velocity layer in the bottom of the crust with varying thicknesses from several to up to 20 km [Wolf and Cipar, 1993]. The upper boundary of this layer represents an approximately 10% increase in V_p , which ranges from 6.8 to 7.3 km/s in the lower crustal layer and is significantly greater than that beneath a typical continental lower crust [Wolf and Cipar, 1993]. We acknowledge that the interpretation of the PACE data and

the existence of a sharp boundary at about 30 km depth are debated [e.g., Parsons *et al.*, 1996].

[49] The petrological nature of the high density mafic lower crustal layer cannot be specified at the present time. One of the possibilities is that the layer is dominantly composed of eclogite and serpentinite. Analyses of eclogite xenoliths found in the Navajo volcanic field located in the NE corner of the study area (Figure 1) suggested that the eclogites represent metamorphosed oceanic lithosphere subducted during Proterozoic subduction [Wendlandt *et al.*, 1993; Selverstone *et al.*, 1999]. However the V_p/V_s of eclogites is 1.785 [Christensen, 1996], which is significantly lower than the observed value of 2.05. The most likely rock that can contribute to such a high V_p/V_s is serpentinite which has an unusually high value of 2.12 [Christensen, 1996] and has been suggested as an explanation for low velocity, high V_p/V_s zones in the mantle wedge above subduction zones [e.g., Bostock *et al.*, 2002; Ranero and Sallares, 2004]. Additionally, coexistence of eclogite and serpentinite was observed in numerous places such as the Voltri Massif in Italy [Cortesogno *et al.*, 1977] and the Dabie-Sulu terrane in China [Jing *et al.*, 2007]. We emphasize that while the evidence for the co-existence of eclogites and serpentinites is convincing, the existence of such a thick layer composed of those rocks beneath the CP remains hypothetical. Additional interdisciplinary studies aimed at resolving this important issue are required to test this hypothesis.

5.4. Implications on the Mechanism Responsible for the Uplift of the CP

[50] As evidenced by the near-horizontal Phanerozoic sedimentary rock strata exposed in the Grand Canyon and elsewhere on the CP, during much of the Phanerozoic until the late Cretaceous, the elevation of the CP was near sea level [Flowers, 2010]. The mechanisms responsible for the uplift of the CP started in Tertiary are one of the major unresolved issues in western U.S. tectonics. It is well established that the CP area is under isostatic equilibrium as revealed by the near-zero free-air gravity anomaly [Keller *et al.*, 1979; Thompson and Zoback, 1979]. Under the reasonable assumption that equilibrium was maintained prior to uplift, the excess mass of the 2 km thick upper-crustal layer must be compensated by an equal amount of mass deficit in the underlying crust and/or mantle.

[51] One group of models for the uplift of CP advocate that the mass deficit is located in the mantle in the form of higher temperature [Roy *et al.*,

2009; *Parsons et al.*, 1996], chemically induced reduction in lithosphere density [*Humphreys et al.*, 2003; *Roy et al.*, 2009], partial replacement of the lithosphere by the lighter asthenosphere [*Spencer*, 1996], or lateral temperature increase in the asthenosphere [*Moucha et al.*, 2009; *West et al.*, 2004].

[52] A competing group of models suggest isostatic uplift due to thickening of the lower crust, and one of the possible mechanisms of such thickening is attributed to the shear stress from the low angle Farallon plate applied on the base of the North American lithosphere. The stress could transport ductile lower crust from SW to NE direction, resulting in a CP crust that is thicker than a typical continental crust [*Bird*, 1984, 1988; *Beghoul and Barazangi*, 1989; *McQuarrie and Chase*, 2000].

[53] Our RF observations, especially the thick upper crustal layer revealed by the *PuS* phases and the results of gravity modeling (Figure 9), do not support the existence of a thickened lower crust beneath the CP. Instead, they suggest a lower crust with an anomalously high density. Such a high-density lower crust can resolve the long-lasting debate about how an area with such a thick crust could stay at sea level. The main supporting evidence of crustal thickening as the cause of CP uplift came from the observation that at the present time, areas with a crustal thickness of 42 km are significantly higher than sea level, and those at sea level have a crustal thickness of about 30–35 km [*Mooney et al.*, 1998], and thus the preuplift CP crust must be thinner than 42 km [*McQuarrie and Chase*, 2000]. This argument is inconsistent with our results. Simple calculations based on the Airy's hypothesis of isostasy conclude that the surface of an area with densities and thicknesses similar to our results (Figures 8 and 9) is close to sea level, mostly due to the greater lower crust density than that in a standard earth model such as PREM [*Dziewonski and Anderson*, 1981]. Thus the resulting high V_p/V_s and especially the required high density in the lower crust beneath the CP (Figure 9) support the models involving a lower density mantle as the cause of the uplift of the plateau.

5.5. Speculations on the Causes for the Stability of the CP

[54] One of the long-lasting debates on western U.S. tectonics is the enigmatic tectonic stability of the CP. Over the past 500 million years the interior of the CP has escaped both significant compressional (e.g., the Sevier and Laramide orogenies) and Cenozoic extensional tectonic events which created

the BRP on the west and the Rio Grande rift on the east of the CP [*Morgan and Swanberg*, 1985].

[55] The most trivial explanation for the stability is that the CP has a mechanically strong (i.e., cold and thick) lithosphere [*Blackwell et al.*, 1991; *Lee et al.*, 2001]. While most seismic tomography studies concluded that at the present time, the CP has a lithosphere that is about twice as thick as that beneath the BRP [e.g., *West et al.*, 2004], the 100% Cenozoic crustal extension in the latter area suggests a similar preextension thickness between the two areas [*Bird*, 1988]. The similarity in pre-extension lithosphere thickness between the two areas was independently suggested by isotopic studies [*Livaccari and Perry*, 1993]. The velocities of the uppermost mantle beneath the CP and the BRP are similar in some of the seismic tomography studies [e.g., *Bedle and van der Lee*, 2009]. Some more recent studies even suggested that at the present time, the CP lithosphere has a lower velocity than that of the BRP. For instance, using data from USArray and other stations, *Burdick et al.* [2010] suggested that in the top 200 km, the *P* wave velocity beneath the CP is consistently lower than that beneath the BRP (Figure 6). Thus a thick and strong mantle lithosphere may not be the cause of the long-term stability of the CP.

[56] On the basis of our RF and gravity modeling results, we speculate that the mafic, dense, and mechanically strong lower crust is mostly responsible for the long-term tectonic stability of the CP. We further hypothesize that an anomalously strong crust might be responsible for other stable blocks among tectonically active provinces such as the Tarim basin between the Tibetan plateau and Tianshan, and the Sichuan basin on the eastern edge of the Tibetan plateau. RF studies similar to the one presented here should be able to pin point if a strong lower crust or a strong mantle lithosphere is responsible for the tectonic stability of those blocks.

6. Conclusions

[57] This study confirmed previously proposed systematic spatial variations in crustal thickness, V_p/V_s and the efficiency of the crust/mantle boundary in producing *P*-to-*S* converted phases across the southwestern Colorado Plateau and the southern Basin and Range Province. The Basin and Range Province is characterized by a thin crust with a V_p/V_s that is similar to a typical cratonic crust, suggesting that crustal thinning was the result of simple stretching of the original crust rather than other processes

such as lower crustal delamination or horizontal transferring of lower crustal material. In contrast, the Colorado Plateau has a mafic crust with a felsic upper crust of about 30 km thick and a mafic lower crust of about 12 km. We hypothesize that the mechanically strong lower crust is responsible for the long-term stability of the CP, and the higher-than-normal density of the lower crust is responsible for the near sea level elevation prior to the Cenozoic uplift of the plateau.

Acknowledgments

[58] Data used for the study were recorded by seismic stations in the USArray network, and several portable seismic experiments. We thank the IRIS DMC for providing the data sets, and M. G. Abdelsalam, G. R. Keller, and R. C. Laudon for fruitful discussions. Constructive reviews by G. R. Keller, an anonymous reviewer, and editor T. Becker significantly improved the manuscript. The study was partially supported by National Science Foundation awards EAR-0703359 and EAR-0952064, and by a University of Missouri Research Board Award. This article is Missouri University of Science and Technology Geology and Geophysics contribution 27.

References

- Aiken, C. (1976), The analysis of the gravity anomalies of Arizona, Ph.D. dissertation, 127 pp., Univ. of Ariz., Tucson.
- Ammon, C. J. (1991), The isolation of receiver effects from teleseismic *P*-wave-forms, *Bull. Seismol. Soc. Am.*, *81*, 2504–2510.
- Bache, T. C., W. L. Rodi, and D. G. Harkrider (1978), Crustal structures inferred from Rayleigh-wave signatures of NTS explosions, *Bull. Seismol. Soc. Am.*, *68*, 1399–1413.
- Bedle, H., and S. van der Lee (2009), *S* velocity variations beneath North America, *J. Geophys. Res.*, *114*, B07308, doi:10.1029/2008JB005949.
- Beghoul, N., and M. Barazangi (1989), Mapping high *Pn* velocity beneath the Colorado Plateau constrains uplift models, *J. Geophys. Res.*, *94*, 7083–7104.
- Bennett, V. C., and D. J. DePaolo (1987), Proterozoic crustal history of the western United States as determined by Nd isotopic mapping, *Geol. Soc. Am. Bull.*, *99*, 674–685.
- Bensen, G. D., M. H. Ritzwoller, and Y. Yang (2009), A 3-D shear velocity model of the crust and uppermost mantle beneath the United States from ambient seismic noise, *Geophys. J. Int.*, *177*, 1177–1196.
- Bird, P. (1979), Continental delamination and the Colorado Plateau, *J. Geophys. Res.* *84*, 7561–7571.
- Bird, P. (1984), Laramide crustal thickening event in the Rocky Mountain Foreland and Great Plains, *Tectonics*, *3*, 741–758.
- Bird, P. (1988), Formation of the Rocky Mountains, western United States: A continuum computer model, *Science*, *239*, 1501–1507.
- Blackwell, D. D., J. L. Steele, and L. S. Carter (1991), Heat-flow patterns of the North American continent; a discussion of the geothermal map of North America, in *Neotectonics of North America*, edited by D. B. Slemmons et al., pp. 423–436, Geol. Soc. of Am., Boulder, Colo.
- Bond, G. (1976), Evidence for continental subsidence in North America during the Late Cretaceous global submergence, *Geology*, *4*, 557–560.
- Bostock, M. G., R. D. Hyndman, S. Rondenay, and S. M. Peacock (2002), An inverted continental *Moho* and serpentinization of the forearc mantle, *Nature*, *417*, 536–538.
- Buehler, J. S., and P. M. Shearer (2010), *Pn* tomography of the western United States using USArray, *J. Geophys. Res.*, *115*, B09315, doi:10.1029/2009JB006874.
- Burdick, S., R. D. Hilst, F. L. Vernon, V. Martynov, T. Cox, J. Eakins, G. H. Karasu, J. Tylell, L. Astiz, and G. L. Pavlis (2010), Model update January 2010: Upper mantle heterogeneity beneath North America from traveltimes tomography with global and USArray transportable array data, *Seismol. Res. Lett.*, *81*, doi:10.1785/gssrl.81.5.689.
- Cady, J. (1980), Calculation of gravity and magnetic anomalies of finite-length right polygonal prisms, *Geophysics*, *45*, 1507–1512.
- Chase, C. G., J. A. Libarkin, and A. J. Sussman (2002), Colorado Plateau: Geoid and means of isostatic support, *Inter. Geol. Rev.*, *44*, 575–587.
- Christensen, N. I. (1996), Poisson's ratio and crustal seismology, *J. Geophys. Res.*, *101*, 3139–3156.
- Christensen, N. I., and W. D. Mooney (1995), Seismic velocity structure and composition of the continental crust: A global view, *J. Geophys. Res.*, *100*, 9761–9788.
- Condie, K. C., and J. Selverstone (1999), The crust of the Colorado Plateau: New views of an Old Arc, *Geology*, *107*, 387–397.
- Coney, P. J., and T. A. Harms (1984), Cordilleran metamorphic core complexes: Cenozoic extensional relics of Mesozoic compression, *Geology*, *12*, 550–554.
- Cortesogno, L., W. G. Ernst, M. Galli, B. Messiga, G. P. Pedemonte, and G. B. Piccardo (1977), Chemical petrology of eclogitic lenses in serpentinite, Gruppo Di Voltri, Ligurian Alps, *J. Geology*, *85*, 255–277.
- Diment, W. H., S. W. Stewart, and J. C. Roller (1961), Crustal structure from Nevada Test Site to Kingman, Arizona, from seismic and gravity observations, *J. Geophys. Res.*, *66*, 201–214.
- Dziewonski, A. M., and D. L. Anderson (1981), Preliminary reference Earth model, *Phys. Earth Planet. Inter.*, *25*, 297–356.
- Efron, B., and R. Tibshirani (1986), Bootstrap methods for standard errors, confidence intervals, and other measures of statistical accuracy, *Stat. Sci.*, *1*, 54–77.
- England, P. C., and G. A. Houseman (1988), The mechanics of the Tibetan Plateau, *R. Soc. London Philos. Trans.*, *326*, 301–319.
- Esperanca, S., W. C. Richard, B. S. Steven and D. Smith (1997), Dating crust-mantle separation: Re-Os isotopic study of mafic xenoliths from central Arizona, *Geology*, *25*, 651–654.
- Flowers, R. M. (2010), The enigmatic rise of the Colorado Plateau, Research Focus, *Geology*, *38*, 671–672.
- Flowers, R. M., B. P. Wernicke, and K. A. Farley (2008), Unroofing incision and uplift history of the southwestern Colorado Plateau from (U-Th)/He apatite thermochronometry, *Geol. Soc. Am. Bull.*, *120*, 571–587.
- Frassetto, A., H. Gilbert, G. Zandt, S. Beck, and M. J. Fouch (2006), Support of high elevation in the southern Basin and Range based on the composition and architecture of the crust in the Basin and Range and Colorado Plateau, *Earth Planet. Sci. Lett.*, *249*, 62–73.
- Gans, P. B., and W. A. Bohrson (1998), Suppression of volcanism during rapid extension in the Basin and Range Province, United States, *Science*, *279*, 66–68.

- Gao, S., B. R. Zhang, Z. M. Jin, H. Kern, T. C. Luo, and Z. D. Zhao (1998), How mafic is the lower continental crust?, *Earth Planet. Sci. Lett.*, *106*, 101–107.
- Gao, S. S., K. H. Liu, and C. Chen (2004), Significant crustal thinning beneath the Baikal rift zone: New constraints from receiver function analysis, *Geophys. Res. Lett.*, *31*, L20610, doi:10.1029/2004GL020813.
- Gilbert, H., A. A. Velasco, and G. Zandt (2007), Preservation of Proterozoic terrane boundaries within the Colorado Plateau and implications for its tectonic evolution, *Earth Planet. Sci. Lett.*, *258*, 237–248.
- Gish, D. M., G. R. Keller, and M. L. Sbar (1981), A refraction study of deep crustal structure in the Basin and Range: Colorado Plateau of eastern Arizona, *J. Geophys. Res.*, *86*, 6029–6038.
- Hauser, C., and J. Lundy (1989), COCORP deep reflections: Moho at 50 km (16 s) beneath the Colorado Plateau, *J. Geophys. Res.*, *94*, 7071–7081.
- Hauser, C., J. Gephart, T. Latham, J. Oliver, S. Kaufman, L. Brown, and I. Lucchitta (1987), COCORP Arizona transect: Strong crustal reflections and offset Moho beneath the transition zone, *Geology*, *15*, 1103–1106.
- Hendricks, J. D., and J. B. Plescia (1991), A review of the regional geophysics of the Arizona transition zone, *J. Geophys. Res.*, *96*, 12,351–12,373.
- Hinojosa, J., and K. Mickus (2002), Finite difference modeling of lithospheric uplifts, *Comput. Geosci.*, *28*, 155–167.
- Holbrook, W. S., W. D. Mooney, and N. I. Christensen (1992), The seismic velocity structure of the deep continental crust, in *Continental Lower Crust*, edited by D. M. Fountain, R. Arculus, and R. W. Kay, pp. 21–43, Elsevier, New York.
- Howard, K. A. (1991), Intrusion of horizontal dikes: Tectonic significance of middle Proterozoic diabase Sheets widespread in the upper crust of the southwestern United States, *J. Geophys. Res.*, *96*, 12,461–12,478.
- Howard, K., and B. John (1987), Crustal extension along a rooted system of imbricate low-angle faults: Colorado River Extensional Corridor, California and Arizona, in *Continental Extensional Tectonics*, edited by M. Coward, *Geol. Soc. London Spec. Publ.*, *28*, 299–311.
- Humphreys, E., E. Hessler, K. Dueker, G. L. Farmer, E. Erslev, and T. Atwater (2003), How Laramide-Age hydration of North American lithosphere by the Farallon slab controlled subsequent activity in the western United States, *Inter. Geol. Rev.*, *45*, 575–595.
- Jing, J., W. Wei, S. Jin, G. Ye, and M. Deng (2007), A study on the classification and well-logging identification of eclogite in the main hole of Chinese Continental Scientific Drilling Project, *J. China Univ. Geosci.*, *18*, 357–365, doi:10.1016/S1002-0705(08)60017-5.
- Jull, M., and P. B. Kelemen (2001), On the conditions for lower crustal convective instability, *J. Geophys. Res.*, *106*, 6423–6446.
- Karlstrom, K. E., and S. A. Bowring (1988), Early Proterozoic assembly of tectono-stratigraphic terranes in southwestern North America, *J. Geol.*, *96*, 561–576.
- Karlstrom, K. E., and E. D. Humphreys (1998), Persistent influence of Proterozoic accretionary boundaries in the tectonic evolution of southwestern North America: Interaction of cratonic grain and mantle modification events, *Rocky Mt. Geol.*, *33*, 161–179.
- Keller, G. R., L. W. Braile, and P. Morgan (1979), Crustal structure, geophysical models and contemporary tectonism of the Colorado Plateau, *Tectonophysics*, *61*, 131–147.
- Kennett, B. L. N., and E. R. Engdahl (1991), Traveltimes for global earthquake location and phase identification, *Geophys. J. Int.*, *105*, 429–465.
- Kennett, B. L. N., E. R. Engdahl, and R. Buland (1995), Constraints on seismic velocities in the Earth from traveltimes, *Geophys. J. Int.*, *122*, 108–124.
- Lachenbruch, A. H., and J. H. Sass (1978), Models of an extending lithosphere and heat flow in the Basin and Range province, in *Cenozoic Tectonics and Regional Geophysics of the Western Cordillera*, edited by R. B. Smith and G. P. Eaton, *Geol. Soc. Am. Mem.*, *152*, 209–250.
- Langston, C. A., and D. V. Helmberger (1974), Interpretation of body and Rayleigh waves from NTS to Tucson, *Bull. Seismol. Soc. Am.*, *64*, 1919–1929.
- Lee, C. T., Q. Yin, R. L. Rudnick, and S. B. Jacobsen (2001), Preservation of ancient and fertile lithospheric mantle beneath the southwestern United States, *Nature*, *411*, 69–73.
- Liu, K. H. (2009), NA-SWS-1.1: A uniform database of teleseismic shear-wave splitting measurements for North America, *Geochem. Geophys. Geosyst.*, *10*, Q05011, doi:10.1029/2009GC002440.
- Liu, K. H., and S. S. Gao (2010), Spatial variations of crustal characteristics beneath the Hoggar swell, Algeria revealed by systematic analyses of receiver functions from a single seismic station, *Geochem. Geophys. Geosyst.*, *11*, Q08011, doi:10.1029/2010GC003091.
- Liu, L., and M. Gurnis (2010), Dynamic subsidence and uplift of the Colorado Plateau, *Geology*, *38*, 663–666.
- Livaccari, R. F., and F. V. Perry (1993), Isotopic evidence for preservation of Cordilleran lithospheric mantle during the Sevier-Laramide orogeny, western United States, *Geology*, *21*, 719–722.
- McCarthy, J., S. P. Larkin, G. S. Fuis, R. W. Simpson, and K. A. Howard (1991), Anatomy of a metamorphic core complexes: Seismic refraction/wide-angle reflection profiling in southeastern California and western Arizona, *J. Geophys. Res.*, *96*, 12,259–12,291.
- McCarthy, J., W. Kohler, and E. Criley (1994), Data Report for the PACE 1989 seismic refraction survey, Northern Arizona, *Open File Rep.*, *94-138*.
- McGuire, A. V. (1994), Southern Basin and Range province crust-mantle boundary evidence from gabbroic xenoliths, Wikieup, Arizona, *J. Geophys. Res.*, *99*, 24,263–24,273.
- McQuarrie, N., and C. G. Chase (2000), Raising the Colorado Plateau, *Geology*, *28*, 91–94.
- Menges, C., and P. Peartree (1989), Late Cenozoic tectonism in Arizona and its impact of regional landscape evolution, in *Geological Evolution of Arizona*, edited by J. Jenny and S. Reynolds, *Ariz. Geol. Soc. Dig.*, *17*, 649–679.
- Mickus, K. (1989), Backus and Gilbert inversion of two and one-half dimensional gravity and magnetic anomalies and crustal structure studies in western Arizona, and the eastern Mojave Desert, California, Ph.D. dissertation, 212 pp., Univ. of Tex. at El Paso.
- Mickus, K., and W. James (1991), Regional gravity studies in southeastern California, western Arizona and southern Nevada, *J. Geophys. Res.*, *96*, 12,333–12,350.
- Mooney, W., G. Laske, and T. Masters (1998), Crust 5.1: A global crustal model at 5°5, *J. Geophys. Res.*, *103*, 727–747.
- Morgan, P., and C. A. Swanberg (1985), On the Cenozoic uplift and tectonic stability of the Colorado Plateau, *J. Geodyn.*, *3*, 39–63.
- Moschetti, M. P., M. H. Ritzwoller, F. Lin, and Y. Yang (2010), Seismic evidence for widespread western-US deep-crustal deformation caused by extension, *Nature*, *464*, 885–890.

- Moucha, R., A. M. Forte, D. B. Rowley, J. X. Mitrovica, N. A. Simmons, and S. P. Grand (2009), Deep mantle forces and the uplift of the Colorado Plateau, *Geophys. Res. Lett.*, *36*, L19310, doi:10.1029/2009GL039778.
- Nair, S. K., S. S. Gao, K. H. Liu, and P. G. Silver (2006), Southern African crustal evolution and composition: Constraints from receiver function studies, *J. Geophys. Res.*, *111*, B02304, doi:10.1029/2005JB003802.
- Parsons, T., J. McCarthy, W. M. Kohler, C. J. Ammon, H. M. Benz, J. A. Hole, and E. E. Criley (1996), Crustal structure of the Colorado Plateau, Arizona: Application of new long-offset seismic data analysis techniques, *J. Geophys. Res.*, *101*, 11,173–11,194.
- Press, W. H., S. A. Teukolsky, W. T. Vetterling, and B. P. Flannery (1996), *Numerical Recipes in FORTRAN 90: The Art of Parallel Scientific Computing*, 2nd ed., Cambridge Univ. Press, New York.
- Prodehl, C. (1979), Crustal structure of the western United States, *U.S. Geol. Surv. Prof. Pap.*, 1034–1074.
- Ranero, C. R., and V. Sallares (2004), Geophysical evidence for hydration of the crust and mantle of the Nazca plate during bending at the north Chile trench, *Geology*, *32*, 549–552.
- Roller, J. C. (1965), Crustal structure in the eastern Colorado Plateau province from seismic-refraction measurements, *Bull. Seismol. Soc. Am.*, *55*, 107–119.
- Roy, M., S. Kelley, F. Pazzaglia, S. Cather, and M. House (2004), Middle Tertiary buoyancy modification and its relationship to rock exhumation, cooling, and subsequent extension at the eastern margin of the Colorado Plateau, *Geology*, *32*, 925–928.
- Roy, M., T. H. Jordan, and J. Pederson (2009), Colorado Plateau magmatism and uplift by warming of heterogeneous lithosphere, *Nature*, *459*, 978–982.
- Sahagian, D., A. Proussevitch, and W. Carlson (2002), Timing of Colorado Plateau uplift: Initial constraints from vesicular basalt-derived paleoelevations, *Geology*, *30*, 807–810.
- Saleeby, J. (2003), Segmentation of the Laramide slab-evidence from the southern Sierra Nevada region, *Geol. Soc. Am. Bull.*, *115*, 655–668.
- Selverstone, J., A. Pun, and K. C. Condie (1999), Xenolithic evidence for Proterozoic crustal evolution beneath the Colorado Plateau, *Geol. Soc. Am. Bull.*, *111*, 590–606.
- Sheehan, A. F., C. H. Jones, M. K. Savage, S. Ozalaybey, and J. M. Schneider (1997), Contrasting lithospheric structure between the Colorado Plateau and Great Basin, Initial results from Colorado Plateau - Great Basin PASSCAL experiment *Geophys. Res. Lett.*, *24*, 2609–2612.
- Sinno, Y. A., G. R. Keller, and M. L. Sbar (1981), A crustal seismic refraction study in west-central Arizona, *J. Geophys. Res.*, *86*, 5023–5038.
- Sonder, L. J., and C. H. Jones (1999), Western United States extension: How the west was widened, *Ann. Rev. Earth Planet. Sci.*, *27*, 417–462.
- Spencer, J. E. (1996), Uplift of the Colorado Plateau due to lithosphere attenuation during Laramide low-angle subduction, *J. Geophys. Res.*, *101*, 13,595–13,609.
- Sumner, J. (1989), Regional geophysics of Arizona, in *Geological Evolution of Arizona*, edited by J. Jenny and S. Reynolds, *Ariz. Geol. Soc. Dig.*, *17*, 717–739.
- Tarkov, A. P., and V. V. Vavakin (1982), Poisson's ratio behavior in various crystalline rocks: Application to the study of the Earth's interior, *Phys. Earth Planet. Inter.*, *29*, 24–29.
- Thompson, G. A., and M. L. Zoback (1979), Regional geophysics of the Colorado Plateau, *Tectonophysics*, *61*, 149–181.
- Van Schmus, W. R., M. E. Bickford, and A. Turek (1996), Proterozoic geology of the east-central Midcontinent basement, in *Basement and Basins of Eastern North America*, edited by B. A. van der Pluijm and P. A. Catacosinos, *Geol. Soc. Am. Spec. Pap.*, *308*, 7–32.
- Warren, D. H. (1969), A seismic-refraction survey of crustal structure in central Arizona, *Geol. Soc. Am. Bull.*, *80*, 257–282.
- Watts, A. (2001), *Isostasy and Flexure of the Lithosphere*, 485 pp., Cambridge Univ. Press, New York.
- Wendlandt, E., D. J. DePaolo, and W. S. Baldrige (1993), Nd and Sr isotope chronostratigraphy of Colorado Plateau lithosphere: Implications for magmatic and tectonic underplating of the continental crust, *Earth Planet. Sci. Lett.*, *116*, 23–43.
- Wernicke, B., G. J. Axen, and J. K. Snow (1988), Basin and Range extensional tectonics at the latitude of Las Vegas, Nevada, *Geol. Soc. Am. Bull.*, *100*, 1738–1757.
- Wessel, P., and W. H. F. Smith (1991), Free software helps map and display data, *Eos Trans. AGU*, *72*, 441.
- West, M., J. Ni, W. S. Baldrige, D. Wilson, R. Aster, W. Gao, and S. Grand (2004), Crust and upper mantle shear wave structure of the southwest United States: Implications for rifting and support for high elevation, *J. Geophys. Res.*, *109*, B03309, doi:10.1029/2003JB002575.
- Whitmeyer, S. J., and K. E. Karlstrom (2007), Tectonic model for the Proterozoic growth of North America, *Geosphere*, *34*, 220–259.
- Wilson, D., J. Leon, R. Aster, J. Ni, S. Grand, S. Semken, W. Gao, and W. S. Baldrige (2002), Broadband seismic background noise at temporary seismic stations observed on a regional scale in the southwestern United States, *Bull. Seismol. Soc. Am.*, *92*, 3335–3341.
- Wilson, D., R. Aster, J. Ni, S. Grand, M. West, W. Gao, W. S. Baldrige, and S. Semken (2005), Imaging the seismic structure of the crust and upper mantle beneath the Great Plains, Rio Grande Rift, and Colorado Plateau using receiver functions, *J. Geophys. Res.*, *110*, B05306, doi:10.1029/2004JB003492.
- Wilson, D., R. Aster, S. Grand, J. Ni, and W. S. Baldrige (2010), High-resolution receiver function imaging reveals Colorado Plateau lithospheric architecture and mantle-supported topography, *Geophys. Res. Lett.*, *37*, L20313, doi:10.1029/2010GL044799.
- Wilson, J. M., and G. S. Fuis (1987), PACE seismic refraction survey report, southern California and western Arizona, *Open File Rep.*, 87-86.
- Wolf, L. W., and J. J. Cipar (1993), Through thick and thin: A new model for the Colorado Plateau from seismic refraction data from Pacific to Arizona Crustal Experiment, *J. Geophys. Res.*, *98*, 19,881–19,894.
- Wolfe, J. A., C. E. Forest, and P. Molnar (1998), Paleobotanical evidence of Eocene and Oligocene paleoaltitudes in mid-latitude western North America, *Geol. Soc. Am. Bull.*, *110*, 664–678.
- Wooden, J. L., and E. DeWitt (1991), Pb isotopic evidence for the boundary between the early Proterozoic Mojave and central Arizona crustal provinces in western Arizona, *Ariz. Geol. Soc. Dig.*, *19*, 27–50.
- Zandt, G., S. C. Myers, and T. C. Wallace (1995), Crust and mantle structure across the Basin and Range–Colorado Plateau boundary at 37°N latitude and implications for Cenozoic extensional mechanism, *J. Geophys. Res.*, *100*, 10,529–10,548.
- Zhu, L. P., and H. Kanamori (2000), Moho depth variation in southern California from teleseismic receiver functions, *J. Geophys. Res.*, *105*, 2969–2980.